Available online at www.sciencedirect.com

ScienceDirect

Procedia Engineering 103 (2015) 197 – 204

Procedia Engineering

www.elsevier.com/locate/procedia

The 13th Hypervelocity Impact Symposium

Momentum Transfer in Hypervelocity Impact Experiments on Rock Targets

Tobias Hoerth[a]*, Frank Schäfer[a], Jan Hupfer[a], Oliver Millon[a] and Matthias Wickert[a]

[a]*Fraunhofer EMI, Eckerstraße 4, 79104 Freiburg, Germany*

Abstract

A special phenomenon observed in hypervelocity impacts on rock targets is the so-called momentum multiplication, i.e. the momentum transferred to the target is greater than the original momentum of the projectile. This effect is caused by ejection of debris in the direction opposite to the flight direction of the projectile. In the present study momentum multiplication was investigated as a function of target material properties and projectile velocity. Hypervelocity impact experiments on target materials with different porosities were conducted and the momentum transfer was measured using a ballistic pendulum.

Low porous materials like quartzite show larger momentum multiplication than porous materials like sandstone. The smallest momentum multiplication was measured for highly porous aerated concrete. Higher projectile velocity leads to higher momentum multiplication. Furthermore, this increase is stronger for low porous materials compared with porous materials.

These observations can be explained by the different ejection behavior. Low porous materials show a directional and very fast ejection whereas porous materials show a slower ejection. The highly porous material shows a diffuse ejection behavior. Furthermore, cratering efficiency is reduced in porous targets leading to a smaller amount of ejected debris. This effect is attributed to energy dissipation caused by irreversible crushing of pore space.

Peer-review under responsibility of the Curators of the University of Missouri On behalf of the Missouri University of Science and Technology

Keywords: Hypervelocity impact experiments, momentum multiplication, porosity

1. Introduction

Hypervelocity impacts into solid brittle materials like rocks are generally characterized by a significant amount of debris ejected backwards. This process causes an effect called “momentum multiplication”, i.e. the change in target momentum after the impact is greater than the original momentum of the impactor. For a given impactor, the ejection characteristics as well as the crater formation process strongly depend on the target material properties. Cratering is less efficient in porous targets compared with non-porous targets due to energy dissipation caused by irreversible pore crushing [1]. Furthermore, porosity influences ejecta dynamics. A steeper ejection is observed for less porous targets [2]. In addition, porous materials show lower ejection velocities [3]. Craters formed in highly porous materials show very deep craters [4-7] due to a different crater formation process that is governed by compaction of target material [3].

Momentum multiplication is an important physical effect because hypervelocity impacts can significally change the orbit of a target. The kinetic impactor concept, i.e. the deflection of a potentially hazardous Near Earth Object (NEO) by an impactor spacecraft, makes use of the momentum multiplication. NEOs cover a broad range of porosities and strengths [8]. In this context, impact experiments at laboratory scale are an important means for the investigation of the influence of target material properties on the momentum imparted to the target. Furthermore, the use of different projectile velocities permits

* Tobias Hoerth. Tel.: +49-761-2714-394; fax: +49-761-2714-1394.
E-mail address: tobias.hoerth@emi.fraunhofer.de

Peer-review under responsibility of the Curators of the University of Missouri On behalf of the Missouri University of Science and Technology
doi:10.1016/j.proeng.2015.04.027

the investigation of scaling effects. Momentum transfer measurements during hypervelocity impact experiments were carried out in numerous studies in the past and are still a subject of intensive research today. Target materials like mortar [9-12], ice [13] and basalt [12] were used. Furthermore, scale size effects in momentum multiplication were studied by Walker et al. [14-15] and numerical studies were conducted by Walker and Chocron [16] and Jutzi and Michel [17].

In the present study hypervelocity impact experiments were conducted to measure the momentum transfer as a function of target material properties and projectile velocity for three different rock types and a highly porous aerated concrete. The ejection behavior was analyzed using high-speed measurement technique. In addition, impact crater volumes were measured to determine the cratering efficiency.

2. Theory

2.1. Momentum multiplication

The efficiency of the momentum transfer is generally expressed by a dimensionless quantity called "momentum multiplication factor β" which denotes the ratio of the change in target momentum after the impact and the momentum of the projectile

$$\beta = \frac{\Delta p_t}{p_p} = \frac{p_p + p_e}{p_p} = 1 + \frac{p_e}{p_p} \tag{1}$$

where p_t denotes the target momentum and p_e and p_p denote the ejecta momentum and the projectile momentum, respectively. For perfectly plastic impacts, i.e. no ejecta is generated, β equals one. However, for impacts into solid, brittle materials like rocks, β can be greater than one due to the ejection process. Thus, for a given impactor momentum, β depends on the mass and velocity of the ejected material. For strength-dominated cratering Holsapple and Housen [18] give the following scaling relation

$$\beta - 1 \sim \left(v_p \cdot \sqrt{\frac{\rho_t}{Y_t}} \right)^{3\mu-1} \cdot \left(\frac{\rho_t}{\rho_p} \right)^{1-3\nu} \tag{2}$$

where v_p denotes the projectile velocity and ρ_t and Y_t denote the target density and the target strength (uniaxial compressive strength, see chapter 3), respectively. The scaling parameter μ is to be determined by means of a power law fit. This parameter is between μ=1/3 (momentum scaling) and μ=2/3 (energy scaling) and depends on the target material properties [19], i.e. μ decreases with increasing porosity: For non-porous materials μ is about 0.55 and ranges from 1/3 to 0.4 for highly porous materials [20]. Equation (2) shows that μ governs the rate of increase of β with increasing projectile velocity. Thus, a steeper increase is expected for low porous target materials. The second term on the right side of Equation (2), often called π_4, accounts for the ratio of target density ρ_t and projectile density ρ_p. The exponent ν is about 0.4 for most target materials [20].

It is important to note that only the ejecta particles that leave the target contribute to $\beta > 1$. Holsapple and Housen [18] give an additional term accounting for the escape velocity which in turn depends on the target. In the horizontal impact experiments conducted in the present study even the slowest ejecta particles leave the target. Thus, the escape velocity is not considered in the following.

Furthermore, scaling up to large asteroids requires the calculation of strength reduction for increasing target size as shown in [18]. In their present form our results apply to impact events at smaller scales. The scope of the present study is to show the principle influence of target material properties and projectile velocity on the momentum multiplication.

2.2. Cratering efficiency

Holsapple [19] gives scaling laws for strength-dominated impact cratering using dimensionless π-values. The "cratering efficiency", often called π_V, is defined as the following ratio

$$\pi_V = \frac{V \rho_t}{m_p} \tag{3}$$

where V denotes the crater volume and m_p denotes the projectile mass. For porous materials, where a significant amount of the crater volume can be formed by compaction of pore space, the numerator in Equation (3) is generally greater than the ejected mass.
The cratering efficiency π_V is plotted against the strength-term

$$\pi_3 = \frac{Y_t}{\rho_t v_p^2} \tag{4}$$

and the π_4-term shown above leading to the following expression

$$\frac{V\rho_t}{m_p} \sim \left(\frac{\rho_t v_p^2}{Y_t}\right)^{\frac{3\mu}{2}} \left(\frac{\rho_t}{\rho_p}\right)^{1-3\nu} \tag{5}$$

3. Experimental methods

The impact experiments were conducted at the "Space Light Gas Gun" (SLGG), a two-stage light-gas accelerator at Fraunhofer EMI in Freiburg, Germany. Aluminum spheres with a diameter of 5 mm were used as projectiles. The projectile velocities were varied between about 3 km/s and almost 7 km/s. Ambient air pressure in the target chamber was kept constant at about 100 mbar. The experimental parameters are shown in Table 1.

For precise measurement of the momentum transfer, a ballistic pendulum was designed and constructed. A special fast-closing valve was developed which prevents an influence of the unwanted gas exhaust from the gun on the displacement of the pendulum. The target displacement after the impact was measured by means of a laser vibrometer. A high-speed camera (40 kfps) was used to investigate the highly transient ejection process (Figure 1).

In some experiments conducted at the SLGG the valve did not close due to a missing trigger signal. In this case β could not be calculated because of an exaggerated pendulum displacement. However, crater volumes were measured and used for the calculation of the cratering efficiency.

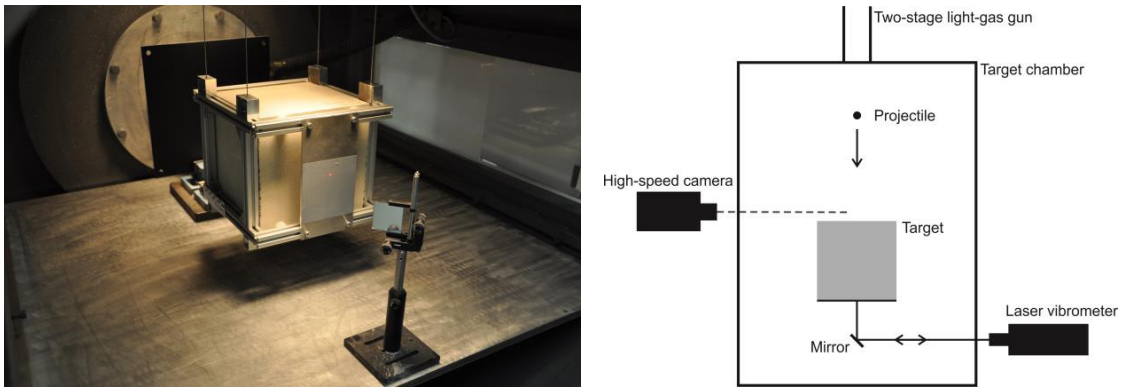

Fig. 1. Experimental set-up within the target chamber. The rock target is attached to a ballistic pendulum. The displacement of the pendulum is measured at the rear surface using a laser vibrometer (red dot is caused by the laser beam). Edge length of the target is 20 cm.

Four different target materials covering a wide range of porosities were used (Table 2). "Wasa-quartzite", the least porous material, is mined in Dalarna, Sweden. A porous sandstone ("Seeberger sandstone") mined in Thuringia, Germany, was used as target material with a moderate porosity (see Poelchau et al. [1] for detailed description of this material). Furthermore, a porous limestone ("Savonnières limestone", mined in Lorraine, France) was used. In addition, highly porous aerated concrete, manufactured in Germany by DOMAPOR, was acquired. The uniaxial compressive strength Y_t (UCS) was determined for all target materials in quasi-static compression tests using cylindrical samples (170 mm x 60 mm) (Table 2).

After the impact experiments 3D-models of all craters were created using a light scanner and crater volumes were measured to calculate the cratering efficiency (Equation (3)).

4. Results and discussion

Figure 2 shows the momentum multiplication factor β as a function of target material and projectile velocity in scaled form (Equation (2)). The results are depicted in Table 1. Two additional data points are added to Figure 2 showing β-values for Yakuno basalt targets [12] with a density and compressive strength of about 2615 kg/m^3 and 160 MPa, respectively [21]. Porosity of Yakuno basalt is about 7 % [22]. These experiments were conducted using 7 mm nylon projectiles at impact velocities of about 2.7 and 3.7 km/s.

The highest β-values are reached for the almost non-porous quartzite (β ≈ 3–4) whereas the highly porous aerated concrete shows the lowest β-values (β ≈ 1.5–2). For all target materials β increases with increasing projectile velocity. A power law of the form $y = a \cdot x^b$ with $b = 3\mu - 1$ was fitted to the data points to determine the material specific scaling exponent μ. For quartzite and limestone only few data points exist so far and no curve fitting was conducted. β-values measured for the porous limestone and for the highly porous aerated concrete show significant scattering.

The quartzite data indicate a steeper increase of β with increasing projectile velocity compared with the porous materials. A power-law fit to the sandstone data leads to $\mu \approx 0.61 \pm 0.04$ which is slightly higher than the values measured by Poelchau et al. [1] ($\mu \approx 0.55 \pm 0.1$) and Hoerth et al. [2] ($0.49 < \mu < 0.56$) for the same kind of sandstone.

A power-law fit to the aerated concrete data leads to $\mu \approx 0.61 \pm 0.09$. Although this value is not very well constrained due to the significant scattering the comparatively large μ-value is somewhat surprising because scaling theory predicts that the dependence of the momentum multiplication factor from projectile velocity decreases with increasing porosity.

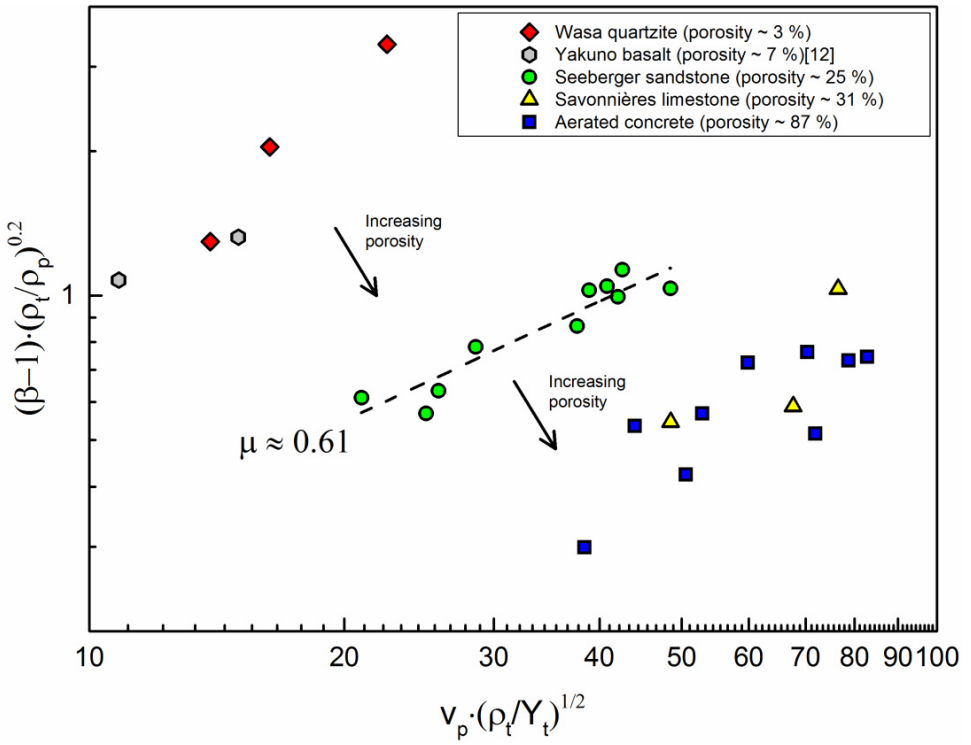

Fig. 2. Momentum multiplication factor β as a function of scaled projectile velocity for different target materials.

For a given impactor momentum the momentum multiplication factor β depends on the mass and velocity of the ejected material (Equation (1)). In Figure 3 the cratering efficiencies are plotted as a function of the strength-term π_3 (Equation (5)). For comparison, quartzite values from Poelchau et al. [23] are also plotted. Higher cratering efficiencies are reached for low-porous quartzites compared with the porous materials. Values taken from Poelchau et al. [23] (Taunus quartzite) agree well with the cratering efficiencies for Wasa quartzite in the present study but lie slightly farther right because the porosity of Taunus quartzite ($\phi \sim 1$ %, [23]) is slightly lower than the porosity of Wasa quartzite ($\phi \sim 3$ %) used in the present study. This reduction in cratering efficiency for porous materials is attributed to energy dissipation caused by crushing of pore space. Again, a power law of the form $y = a \cdot x^b$ with $b = 3\mu/2$ was fitted to the sandstone data leading to a scaling parameter

$\mu = 0.49 \pm 0.09$. In this case μ is slightly lower compared with the values cited above ([1], [2]). For aerated concrete only the experiments conducted at the highest projectile velocities are plotted (Exp. # 5482, 5540 and 5541, see Table 1) because these impacts resulted in rather "bowl-shaped" craters in contrast to the slower projectile velocities where rather thin and very deep "tube-like" craters were formed (Figure 4).

For the porous materials, crater volume is formed both by ejection of material and compaction of pore space. For highly porous materials the crater formation process is described by Kadono [24]. In this model narrow but deep craters are formed for low projectile velocities (no or little breakup of the projectile) whereas at higher projectile velocities (strong projectile breakup) wide craters are formed. In the present study the craters formed in aerated concrete show this behavior and confirm this model. Numerous projectile remnants were found at the crater floor.

For the almost non-porous quartzite the product of crater volume and target density, used for calculation of the cratering efficiency π_V (Equation (3)), agrees well with the ejected mass. For the porous materials, however, and especially for the aerated concrete, this is not the case due to the compaction of pore space as described above. For this reason the amount of ejected material for aerated concrete is smaller than the product of target density and crater volume. However, Figure 3 shows the general trend that higher porosity leads to a reduced cratering efficiency.

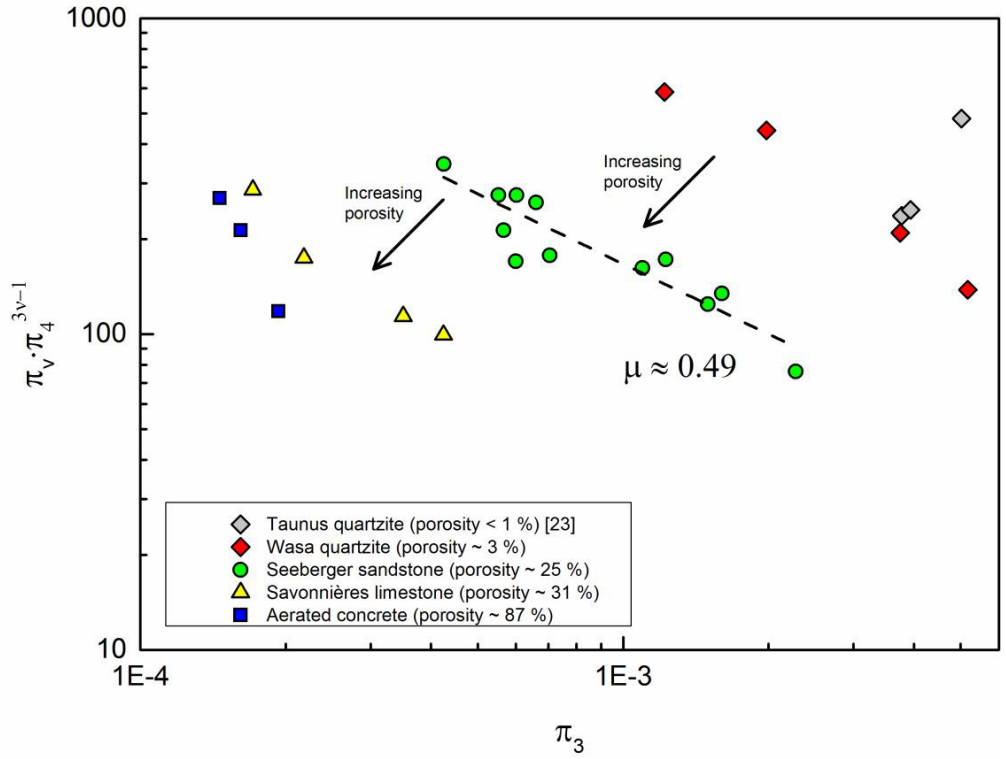

Fig. 3. Strength scaling of experimentally created impact craters.

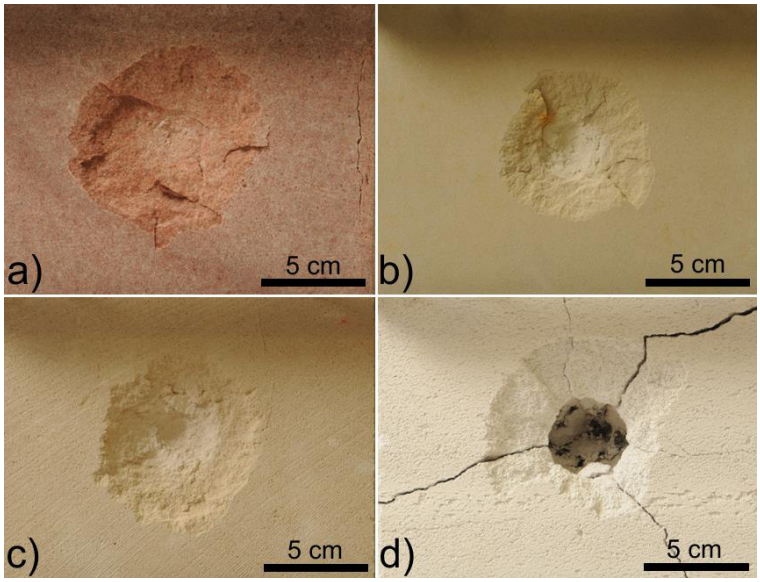

Fig. 4. Impact craters formed in a) quartzite (Exp.# 5480), b) sandstone (Exp.# 5479), c) limestone (Exp.# 5481) and d) aerated concrete (Exp.# 5482). Projectile velocities were about 5.6 km/s (quartzite), 6.1 km/s (sandstone), 6.0 km/s (limestone) and 6.0 km/s (aerated concrete).

For a given projectile velocity and size, ejecta behavior can be significantly different depending on the target material properties. In Figure 5 two consecutive high-speed video frames (40 kfps, 1 µs exposure) for impacts into quartzite, sandstone, limestone and aerated concrete are shown. The experiments were conducted at similar projectile velocities. Quartzite shows a cone-shaped and directional ejection. Sandstone and limestone also show a cone-shaped ejection but the angle between ejecta cone and target surface is smaller for sandstone and even smaller for limestone compared with quartzite. Hence, higher porosity leads to a wider ejecta cone and, thus, to a shallower ejection. Aerated concrete, on the other hand, shows a diffuse ejection behavior and no ejecta cone can be observed. Although ejecta velocities were not measured in the present study a qualitative anlysis shows that the speed of the foremost front of the ejecta cone decreases with increasing porosity. This observation is in accordance with Housen and Holsapple [3] who point out that porous materials show lower ejection velocities.

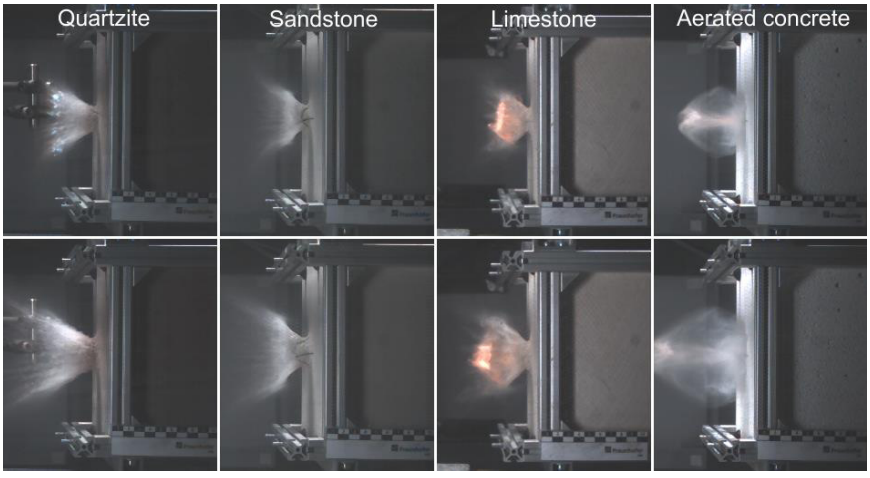

Fig. 5. Comparison between the ejection processes at early stages after the impact for quartzite (Exp. # 5554), sandstone (Exp. # 5548), limestone (Exp. # 5636) and aerated concrete (Exp. # 5537). For each target material two consecutive frames are shown. Frame rate was 40 kfps. Time interval between the two frames is 25 µs. Projectile velocities were about 4.1 km/s (quartzite), 3.7 km/s (sandstone), 3.8 km/s (limestone) and 3.7 km/s (aerated concrete). Scale bar is 10 cm.

The observations shown in the present study lead to a better understanding of the dependence of the momentum multiplication factor β on the target material properties. The higher amount of ejected mass in combination with the faster and steeper ejection (larger normal component with respect to the target surface) observed for low porous targets lead to an enhanced β-value. However, Sommer et al. [25] show that increasing impact velocity leads to a wider ejecta cone (smaller normal component) and, thus, counteracts this process. In this case the higher ejection velocity as well as the larger ejected mass may play the dominant role in momentum multiplication.

Acknowledgments

Density and porosity of the target materials were measured at Albert-Ludwigs Universität Freiburg, Germany. We would like to thank the interns Nico Reichenbach, Dominik Haas and Georg Schäfer for their support in conducting the impact experiments and Hans-Peter Osterer for running the light-gas accelerator. The experiments were conducted in the framework of the NEOShield project which is funded by the Seventh Framework Programme of the European Commission.

References

[1] Poelchau, M. H., Kenkmann, T., Thoma, K., Hoerth, T., Dufresne, A., Schäfer, F., 2013. The MEMIN research unit: Scaling impact cratering experiments in porous sandstones, Meteoritics & Planetary Science 48, pp. 8-22.
[2] Hoerth, T., Schäfer, F., Thoma, K., Kenkmann, T., Poelchau, M. H., Lexow, B., Deutsch, A., 2013. Hypervelocity impacts on dry and wet sandstone: Observations of ejecta dynamics and crater growth. Meteoritics & Planetary Science 48, pp. 23-32.
[3] Housen, K. R. and Holsapple, K. A., 2003. Impact cratering on porous asteroids, Icarus 163, pp. 102-119.
[4] Gault, D. E., Quaide, W. L., Oberbeck, V. R., Moore, H. J., 1966. Luna 9 photographs: Evidence for a fragmental surface layer, Science 153, pp. 985-988.
[5] Love, S. G., Hörz, F., and Brownlee, D. E., 1993. Target porosity effects in impact cratering and collisional disruption. *Icarus* 105, pp. 216-224.
[6] Michikami, T., Moriguchi, K., Hasegawa, S., Fujiwara, A., 2007. Ejecta velocity distribution for impact cratering experiments on porous and low strength targets, Planetary and Space Science 55, pp. 70-88.
[7] Hörz, F., Cintala, M. J., Zolensky, M. E., 1993. Hypervelocity penetration tracks in very low-density, porous targets, in "Hypervelocity impacts in space" J. A. M. McDonnell, Editor. Unit for Space Sciences, University of Kent, Canterbury, pp. 19-23.
[8] Britt, D. T., Yeomans, D., Housen, K., Consolmagno, G., 2002. Asteroid density, porosity, and structure, in *"Asteroids III"* Bottke, W. F., Cellino, A., Paolicchi, P., Binzel, R., Editors. University of Arizona Press, pp. 485-500.
[9] Yanagisawa, M., Eluszkiewicz, J., Ahrens, T. J., 1991. Angular momentum transfer in low velocity oblique impacts: Implications for Asteroids, Icarus 94, pp. 272-282.
[10] Shirono, S., Tada, M., Nakamura, A. M., Kadono, T., Rivkin, A., Fujiwara, A., 1993. Efficiency of linear and angular momentum transfer in oblique impact, Planetary and Space Science 41, pp. 687-692.
[11] Yanagisawa, M., Hasegawa, S., Shirogane, N., 1996. Momentum and angular momentum transfer in oblique impacts: Implications for asteroid rotations, Icarus 123, pp. 192-206.
[12] Yanagisawa, M., and Hasegawa, S., 2000. Momentum transfer in oblique impacts: Implications for asteroid rotations, Icarus 146, pp. 270-288.
[13] Tedeschi, W. J., Remo, J. L., Schulze, J. F., Young, R. P., 1995. Experimental hypervelocity impact effects on simulated planetesimal materials, International Journal of Impact Engineering 17, pp. 837-848.
[14] Walker, J. D., Chocron, S., Durda, D. D., Grosch, D. J., Movshovitz, N., Richardson, D. C., Asphaug, E., 2013. Momentum enhancement from aluminum striking granite and the scale size effect, International Journal of Impact Engineering 56, pp. 12-18.
[15] Walker, J. D., Chocron, S., Durda, D. D., Grosch, D. J., Movshovitz, N., Richardson, D. C., Asphaug, E., 2013. Scale size effect in momentum enhancement, Procedia Engineering 58, pp. 240-250.
[16] Walker, J. D., and Chocron, S., 2011. Momentum enhancement in hypervelocity impact, International Journal of Impact Engineering 38, pp. A1-A7.
[17] Jutzi, M., and Michel, P., 2014. Hypervelocity impacts on asteroids and momentum transfer. I. Numerical simulations using porous targets, Icarus 229, pp. 247-253.
[18] Holsapple, K. A., and Housen, K. R., 2012. Momentum transfer in asteroid impacts. I. Theory and scaling, Icarus 221, pp. 875-887.
[19] Holsapple, K. A., 1993. The scaling of impact processes in planetary sciences, Annu. Rev. Earth Planet. Sci. 21, pp. 333-373.
[20] Holsapple, K. A., and Housen, K. R., 2007. A crater and its ejecta: An interpretation of Deep Impact, Icarus 187, pp. 345-356.
[21] Takagi, Y., Mizutani, H., Kawakami, S., 1984. Impact fragmentation experiments of basalts and pyrophyllites, Icarus 59, pp. 462-477.
[22] Shimada, M., Ito, K., Cho, A., 1989. Ductile behavior of a fine-grained porous basalt at room temperature and pressures to 3 GPa, Physics of the Earth and Planetary Interiors 55, pp. 361-373.
[23] Poelchau, M. H., Kenkmann, T., Hoerth, T., Schäfer, F., Rudolf, M., Thoma, K., 2014. Impact cratering experiments into quartzite, sandstone and tuff: The effects of projectile size and target properties on spallation, Icarus 242, pp. 211-224.
[24] Kadono, T., 1999. Hypervelocity impact into low density material and cometary outburst, Planetary and Space Science 47, pp. 305-318.
[25] Sommer, F., Reiser, F., Dufresne, A., Poelchau, M. H., Hoerth, T., Deutsch, A., Kenkmann, T., Thoma, K., 2013. Ejection behavior characteristics in experimental cratering in sandstone targets, Meteoritics & Planetary Science 48, pp. 33-49.

Appendix A.

Table 1. Impact parameters and results

Exp. #	Target material	Projectile diameter [mm]	Projectile mass [g]	Projectile velocity [m/s]	β	π_V
5480	Quartzite	5	0.177	5570	4.35	444.03
5554	Quartzite	5	0.177	4050	3.05	210.31
5555	Quartzite	5	0.177	7102	-	587.67
5638	Quartzite	5	0.178	3446	2.30	138.84
5473	Sandstone	5	0.177	5870	-	291.09
5474	Sandstone	5	0.177	5602	2.09	275.90
5475	Sandstone	5	0.177	5880	2.11	179.87
5479	Sandstone	5	0.177	6057	2.05	225.61
5543	Sandstone	5	0.177	3597	1.60	142.40
5546	Sandstone	5	0.177	3017	1.65	80.56
5547	Sandstone	5	0.177	4348	-	171.36
5548	Sandstone	5	0.177	3719	1.67	131.66
5549	Sandstone	5	0.177	5423	1.91	187.62
5550	Sandstone	5	0.177	6129	2.20	291.47
5551	Sandstone	5	0.177	6986	2.09	365.66
5553	Sandstone	5	0.177	4112	1.83	182.39
5481	Limestone	5	0.177	6018	2.12	311.35
5634	Limestone	5	0.177	4203	-	123.73
5635	Limestone	5	0.177	5327	1.64	189.43
5636	Limestone	5	0.177	3818	1.59	108.05
5482	Aerated concrete	5	0.177	5993	1.77	176.34
5534	Aerated concrete	5	0.177	4410	1.85	-
5535	Aerated concrete	5	0.177	4217	1.63	-
5537	Aerated concrete	5	0.177	3672	1.80	-
5538	Aerated concrete	5	0.177	5863	2.14	-
5539	Aerated concrete	5	0.177	4991	2.08	-
5540	Aerated concrete	5	0.177	6559	2.10	318.87
5541	Aerated concrete	5	0.177	6897	2.11	403.09
5545	Aerated concrete	5	0.177	3202	1.45	-

Appendix B.

Table 2. Target material properties

Material	Density ρ_t [g/cm^3]	Porosity ϕ [%]	UCS Y_t [MPa]
Wasa quartzite	2.64	2.94	187.6 ± 18.2
Seeberger sandstone	2.04	25.27	42.3 ± 2.4
Savonnières limestone	1.78	31.01	9.8 ± 1.5
Aerated concrete	0.36	87.46	1.8 ± 0.2